WAPD-T-3086

CONF-981003--

COUPLING 2-D CYLINDRICAL AND 3-D X-Y-Z TRANSPORT COMPUTATIONS

I. K. Abu–Shumays, C. E. Yehnert, and T. N. Pitcairn

June 30, 1998

DE-AC11-93PN38195

BETTIS ATOMIC POWER LABORATORY **WEST MIFFLIN, PENNSYLVANIA 15122**

Operated for the U. S. Department of Energy
by WESTINGHOUSE ELECTRIC COMPANY
a division of CBS Corporation

DISCLAIMER

COUPLING 2-D CYLINDRICAL AND 3-D X-Y-Z TRANSPORT COMPUTATIONS

by

I. K. Abu–Shumays, C. E. Yehnert, and T. N. Pitcairn
Bettis Atomic Power Laboratory, P. O. Box 79, West Mifflin, PA 15122-0079

ABSTRACT

This paper describes a new two-dimensional (2-D) cylindrical geometry to three-dimensional (3-D) rectangular x-y-z splice option for multi-dimensional discrete ordinates solutions to the neutron (photon) transport equation. Of particular interest are the simple transformations developed and applied in order to carry out the required spatial and angular interpolations. The spatial interpolations are linear and equivalent to those applied elsewhere. The angular interpolations are based on a high order spherical harmonics representation of the angular flux. Advantages of the current angular interpolations over previous work are discussed. An application to an intricate streaming problem is provided to demonstrate the advantages of the new method for efficient and accurate prediction of particle behavior in complex geometries.

1. Introduction

Programs based on the discrete ordinates method for solving the transport equation over rectangular mesh in r-z cylindrical geometry are used extensively for shield design and analysis. Three-dimensional transport computations are still very expensive for realistic modeling of large shielding problems. Application of 2-D cylindrical geometry models involves conservative approximation and material homogenization techniques. Complex subregions which involve local gaps or nozzles are smeared over rings. The effects of gaps or nozzles are also modeled using axes of symmetry other than the vessel center line. In the past, solutions were obtained through a combination of 2-D models and normalization factors. In situations where local behavior is of interest, designers typically apply hybrid methods which represent the global behavior by an r-z model while the local behavior is treated as accurately as possible by a Monte Carlo solution. Coupling discrete ordinates and Monte Carlo computations has been very effective but expensive, because of the large number of Monte Carlo histories needed to reduce statistical uncertainty.

The present work deals with coupling 2-D cylindrical geometry to 3-D x-y-z geometry discrete ordinates computations. An example is shown in Figure 1 where a secondary 3-D solution space is embedded in a primary 2-D cylindrical problem. Complexities due to different substructures and material compositions are not shown in Figure 1, but are assumed to be present.

The orientation of the axes of the 3-D geometry is arbitrary except for the requirement that one axis of the problem, (x, y, or z) must be parallel to the axis of the cylinder. In addition, the 3-D region need not be totally embedded in the cylindrical region.

Splice options [1, 4-6] have been extensively utilized to break up a very large solution space (which may have excessive memory requirements on the computer system under consideration) into smaller, overlapping regions which are then solved successively with appropriate incident flux boundary conditions. This option has also been widely utilized for sensitivity studies which involve solving a very large primary problem once, saving incident boundary fluxes on faces of a small subregion of a secondary problem of interest, then repeatedly changing compositions, spatial mesh and angular quadratures over the subregion and solving the transport problem over the subregion to study the effects of the various local changes. Linear and averaging type spatial interpolations have been used. Logarithmic interpolations have also been used for the spatial variables [6].

Most of the early work on the splice option with which the current authors are familiar was developed at the Oak Ridge National Laboratory (ORNL) [4-6]. Angular interpolations employed at ORNL are based on so-called "look-backward" and "look-forward" methods.

In the look-backward method, the angular flux along each secondary discrete direction (angular direction of a secondary problem) is equated to the angular flux along the nearest primary discrete direction (angular direction of the primary problem) [6]. This procedure is adequate only when matching angular directions are specified and when the angular flux magnitude varies smoothly over the angular direction space. D. B. Simpson [6] cites examples where the look-backward method is inadequate. For example, this method does not properly treat cases where a fine angular quadrature is used in the primary problem and a coarse angular quadrature is used in a secondary problem. Simpson also states that it is important that the angular quadrature directions in the primary problem have equal weights, since no correction for weight mismatch is available.

In the look-forward method, the angular flux along each incoming direction in a primary problem is mapped into the angular flux along three or less secondary directions for the secondary problem according to the relative nearness. The weights are normalized to preserve net flux values. D. B. Simpson [6] points out situations where the look-forward method is superior to the look-backward method. He also points out that the look-forward method can result in secondary angular fluxes equal to zero along certain directions which are not members of any group of the secondary directions assigned to all of the primary directions. He further states that the likelihood of incorrectly assigning zero angular flux values increases as the ratio of the number of secondary to the number of primary angular directions increases.

While the look-backward and look-forward methods [4-6] proved to be useful for several applications, flexibility in the selection of angular quadratures and accuracy considerations are very important. This report attempts to overcome difficulties with the earlier treatment of angular interpolation. In a recent paper [1], the authors introduced a new method for implementing the splice option for 3-D transport computations. The present paper extends the work in [1] to the splice options for coupling 2-D r-z cylindrical geometry problems to 3-D x-y-z problems.

2. Spherical Harmonic Representation and Related Approximations.

The method of source iterations for multi-groups makes it possible to consider a one energy group transport equation at a time

$$\underline{\Omega} \cdot \overline{\nabla}\Psi(\underline{x}, \underline{\Omega}) + \sigma(\underline{x})\Psi(\underline{x}, \underline{\Omega}) - \sum_{l=0}^{L} \frac{2l+1}{4\pi}\sigma_l^s \sum_{m=-l}^{l} R_{lm}(\underline{\Omega})\phi_{lm} = S(\underline{x}, \underline{\Omega}), \tag{1}$$

where Ψ is the angular flux or particle density at position $\underline{x}$ for particles moving along the angular direction of the unit vector $\underline{\Omega}$, σ is a total cross section, σ_l^s are the Legendre moments of the scattering cross section σ^s, $R_{lm}(\underline{\Omega})$ are spherical harmonics, ϕ_{lm} are spherical harmonics flux moments and $S(\underline{x}, \underline{\Omega})$ is a source term comprised of external sources, fission sources and scattering contributions from other energy groups to the energy group under consideration. The derivation of Eq. (1) involves the assumption that the scattering term from angle $\underline{\Omega}'$ to angle $\underline{\Omega}$ and the angular flux can be expanded in Legendre polynomials and spherical harmonics as

$$\sigma^s(\underline{x}, \underline{\Omega}' \rightarrow \underline{\Omega}) = \sum_{l=0}^{L} \frac{2l+1}{4\pi}\sigma_l^s(\underline{x})P_l(\underline{\Omega}' \cdot \underline{\Omega}), \tag{2}$$

$$\Psi(\underline{x}, \underline{\Omega}) = \sum_{n=0}^{\infty} \frac{2n+1}{4\pi} \sum_{m=-n}^{n} \phi_{nm}(\underline{x})R_{nm}(\underline{\Omega}), \tag{3}$$

where

$$R_{nm}(\underline{\Omega}) \equiv R_{nm}(\mu, \varphi) \equiv \left[\frac{(2-\delta_{m0})(n-m)!}{(n+m)!}\right]^{1/2} P_n^m(\mu)\cos(m\varphi), \tag{4}$$

$$R_{n,-m}(\underline{\Omega}) \equiv R_{n,-m}(\mu,\varphi) \equiv \left[\frac{2(n-m)!}{(n+m)!}\right]^{1/2} P_n^m(\mu)\sin(m\varphi), \qquad m > 0, \tag{5}$$

μ is the cosine of the polar angle as measured from the z-axis, φ is the azimuthal angle as measured from the x-axis in the x-y plane (as measured from the r-axis in a radial plane in cylindrical r-z geometry), δ_{m0} is the Kronecker delta function, and where $P_n^m(\mu)$ are the associated Legendre polynomials. The spherical harmonics moments are given by

$$\phi_{lm}(\underline{x}) = \int_{\Omega} \Psi(\underline{x}, \underline{\Omega})R_{lm}(\underline{\Omega})d\Omega, \tag{6}$$

where the integrals are over the unit sphere.

In production computer programs, the integrals in Eq. (6) required for evaluating the scattering terms in the transport equation are approximated by angular quadratures

$$\phi_{lm}(\underline{x}) \approx \sum_{\tau} \omega_\tau \Psi(\underline{x}, \underline{\Omega}^\tau)R_{lm}(\underline{\Omega}^\tau), \tag{7}$$

where Ω^τ and ω_τ are appropriate quadrature coordinates and weights. The accuracy of the approximation in Eq. (7) for evaluating angular flux moments is a function of the angular quadrature selected. One of the requirements for the construction of angular coordinates and weights is for Eq. (7) to be exact or highly accurate for $0 \le |m| \le l \le 3$. This requirement is

needed to ensure particle balance and to satisfy a diffusion limit. The required accuracy of Eq. (7) is excellent for practical applications which are typically restricted to P_3 scattering (L=3 in Eq. (2)). The approximation in Eq. (7) is exact or highly accurate for higher order scattering representations only for certain angular quadrature selections. The main difficulty is that while the orthogonality property of the spherical harmonics

$$\int_{\Omega} d\Omega \; R_{nk}(\underline{\Omega}) R_{lm}(\underline{\Omega}) = \frac{4\pi}{2n+1} \delta_{nl} \delta_{km}, \tag{8}$$

holds, its numerical approximation by angular quadrature

$$\sum_{\tau} \omega_{\tau} R_{nk}(\underline{\Omega}^{\tau}) R_{lm}(\underline{\Omega}^{\tau}) \approx \frac{4\pi}{2n+1} \delta_{nl} \delta_{km}, \tag{9}$$

is not necessarily valid and can lead to large errors. Consequently, the authors recommended in [1] replacing Eq. (7) by a least squares method, such as is found in LINPACK or LAPACK [2, 3], for evaluating the spherical harmonic moments ϕ_{lm} based directly on Eq. (3) and the angular quadrature selected.

Note that for the special case of cylindrical geometry, assuming rotational invariance, only a hemisphere of angular directions needs to be considered. If the azimuthal angle φ is measured from the r-axis in each radial plane, then it is sufficient to consider the range $\varphi \in [0, \pi]$. For this case, the flux moments ϕ_{lm} , $m < 0$, in Eqs. (1) and (3) associated with the spherical harmonics in Eq. (5) which are odd in φ must vanish. Consequently, the summation over m in the above equations should be restricted to non-negative values $m \geq 0$.

3. Basic Transformations for Spatial and Angular Interpolations.

As mentioned above, the orientation of the axes of the 3-D geometry is arbitrary except for the requirement that one axis of the problem (x, y, or z) must be parallel to the axis of the cylinder. For illustration, assume that the z-axis of the 3-D problem is parallel to the z-axis of the 2-D cylindrical problem, as in Figure 1, and assume that the spatial mesh and angular quadratures for both problems have been defined.

Two fundamental assumptions are made here: (i) all cell-average fluxes are approximately the same as fluxes at the corresponding geometric centers of the cells, and (ii) all cell-face average fluxes are approximately the same as fluxes at the corresponding geometric centers of the cell faces.

Once a primary cylindrical geometry transport problem is solved, the task is to construct incident fluxes on anywhere from one to six faces of a secondary 3-D problem of interest. The required interpolations from the 2-D primary problem to the incident faces of the 3-D secondary problem can be computed more economically in the 2-D cylindrical r-z geometry space than in the 3-D space. An essential task then is to define the spatial and angular transformations from the secondary 3-D x-y-z rectangular geometry to the corresponding primary 2-D r-z cylindrical geometry. Note from Figure 1 that the origin of the 3-D problem is assumed to be located at a height z_1 and at a distance r_1 from the axis in 2-D geometry. In other words:

$$(r_1,\ z_1)_{2\text{-}D} = (0,\ 0,\ 0)_{3\text{-}D}. \tag{10}$$

Similarly, the intersection of the cylindrical axis in 2-D and the x-y plane in 3-D is given by

$$(0,\ z_1)_{2\text{-}D} = (x_c,\ y_c,\ 0)_{3\text{-}D}. \tag{11}$$

The orientation of the 3-D problem relative to the 2-D cylindrical problem (see Figure 1) can be completely defined by specifying height z_1 and either

(i) r_1 and α, where r_1 is the distance between the origin in the 3-D geometry and the axis of the cylinder, and α is the angle (measured counter-clockwise) between the x-axis in 3-D and the r-axis in 2-D, or

(ii) r_1, and r_2, where $(r_1,\ z_1)$ and $(r_2,\ z_1)$ are respectively the coordinates in the r-z system of the origin $(0,\ 0,\ 0)$ and the corner $(0,\ y_{max},\ 0)$ of the 3-D problem.

The size $(x_{max},\ y_{max},\ z_{max})$ of the 3-D problem is needed to identify the region of the 2-D problem over which spatial and angular interpolations are to be performed.

The coordinates x_c, y_c in Eq. (11) of the axis of the cylinder in the x-y plane of the 3-D coordinate system, are given by

$$x_c = -\,r_1 \cos\alpha, \qquad y_c = r_1 \sin\alpha, \tag{12}$$

or by

$$x_c = -\,r_2 \sin\beta, \qquad y_c = y_{max} - r_2 \cos\beta, \tag{13}$$

$$\cos\beta = (y^2_{max} + r_2^{\,2} - r_1^{\,2})/(2r_2 y_{max}), \qquad \sin\beta = \sqrt{1-\cos^2\beta}, \tag{14}$$

where β is the angle between r_2 and the negative y-axis as shown in Figure 1.

Since the actual spatial and angular interpolations are to be carried out in the cylindrical coordinate system, it is necessary to transform $(\underline{x}, \Omega) = (x, y, z, \Omega_x, \Omega_y, \Omega_z)$ from the 3-D system to the 2-D cylindrical system. The required transformations are given by

$$[z, \Omega_z]_{2-D} = [z + z_1, \Omega_z]_{3-D}, \tag{15}$$

$$r = \{(x-x_c)^2 + (y-y_c)^2\}^{1/2}, \tag{16}$$

$$\Omega_r = \frac{\Omega_x(x-x_c) + \Omega_y(y-y_c)}{r}. \tag{17}$$

The direction cosines have different signs in different octants of the unit sphere. In practice, one defines angular ordinates and weights in the first octant of the unit sphere and introduces appropriate signs to account for the angular ordinates and weights in other octants of the unit sphere.

Once the discrete ordinates equations are solved for the 2-D cylindrical problem, the above relations are used as a basis for constructing the angular flux incident on as many as six of the faces of the 3-D problem. In this work, linear interpolations are applied to the space variables and spherical harmonics representations are used for angular interpolations, as is described below.

4. Flux Moment Files, and Spatial and Angular Interpolations.

To employ a 2-D r-z to 3-D x-y-z splice option, a user would typically define the range

$$r_{min} \le r \le r_{max}, \qquad z_{min} \le z \le z_{max}, \qquad (z_{min} \le z_1), \tag{18}$$

in the r-z plane over which the 3-D problem of interest is to be located. The range in Eq. (18) should be large enough to allow the user to apply the splice option to possibly different 3-D secondary problems of interest. Once the r-z problem is solved, a sweep through the mesh is carried out in order to evaluate and save flux moments over the range in Eq. (18). Note again that for r-z geometry, because of symmetry, a truncated form of the expansion Eq. (3) of the angular flux in spherical harmonics reduces to

$$\Psi(\underline{x}, \underline{\Omega}) = \sum_{n=0}^{N} \frac{2n+1}{2\pi} \sum_{m=0}^{n} \phi_{nm}(\underline{x}) R_{nm}(\underline{\Omega}), \tag{19}$$

where spherical harmonics moments are given by

$$\phi_{nm}(\underline{x}) = \int_{-1}^{1} d\mu \int_{0}^{\pi} d\varphi \Psi(\underline{x}, \underline{\Omega}) R_{nm}(\underline{\Omega}) . \tag{20}$$

Note that for a given order N of spherical harmonic expansion in Eq. (19), there are

$$M = (N + 1)(N + 2)/2, \tag{21}$$

flux moments ϕ_{nm}. The choice of N should be such that M is less than or equal to the number of angular quadrature directions corresponding to the 2-D r-z cylindrical problem. For a 2-D angular quadrature with Γ angles per octant, one should select N in Eqs. (19)-(21) such that

$$M \le 4\Gamma. \tag{22}$$

In practice, the computations of the actual flux values are expected to include round off errors and noise. Thus, selecting a value of M smaller than the maximum in Eq. (22) results in general in a smoothing effect.

For certain appropriate choices $\underline{\Omega}^{\tau}$ and ω_{τ} of quadrature coordinates and weights, the flux moments can be reasonably well approximated by

$$\phi_{nm}(\underline{x}) \approx \sum_{\tau} \omega_{\tau} \Psi(\underline{x}, \underline{\Omega}^{\tau}) R_{nm}(\underline{\Omega}^{\tau}). \tag{23}$$

A preferred approach, which would improve accuracy, is to evaluate the flux moments in Eq. (19) by a constrained least squares method [1, 2, 3]. The constraints would be satisfied by evaluating all moments for $0 \le m \le n \le 2$ based on Eq. (23), and by evaluating the higher order moments by requiring Eq. (19) to be satisfied in the least squares sense for known angular flux values at the selected quadrature directions $\underline{\Omega}^{\tau}$. Improved accuracy would result by selecting different ϕ^{+}_{nm} and ϕ^{-}_{nm} least squares flux moments for each of the ranges $0 \le \mu \le 1$, and $-1 \le \mu \le 0$. In this case, since only half of the range of μ is considered at a time, only even functions of μ in the expansion in Eq. (19) need to be retained. In this case

$$\phi^{+}_{nm} = \phi^{-}_{nm} = 0, \qquad for\ n\ odd, \tag{24}$$

and these odd moments need not be computed or stored. For each of the half ranges $0 \le \mu \le 1$, and $-1 \le \mu \le 0$, Eq. (19) reduces to

$$\Psi(\underline{x}, \underline{\Omega}) = \sum_{n=0}^{[N/2]} \frac{4n+1}{\pi} \sum_{m=0}^{2n} \phi^{\gamma}_{2n,m}(\underline{x}) R_{2n,m}(\underline{\Omega}), \qquad \gamma = + \text{ or } \gamma = - . \tag{25}$$

Again, the moments $\phi^{+}_{2n,m}$ and $\phi^{-}_{2n,m}$ in Eq. (25) can be computed based on the quadrature formula Eq. (23) with summation only over the appropriate half range of angles in the upper or lower octants of the unit sphere for $n=0$ and $n=1$, and by least squares for higher values of n.

High order angular quadratures are often required for improved accuracy of practical problems. It has been our experience that M in the range 8 to 14 is appropriate for most applications, as it results in reasonable accuracy and some degree of smoothness.

Once the solution to the primary 2-D problem has converged, the main tasks are the following:

(i) Carry out one sweep through the mesh (for all directions) and evaluate the full ϕ_{nm} or partial ϕ^{+}_{nm} and ϕ^{-}_{nm} flux moments based on least squares as outlined above and described in [1]. This should be done at all mesh cell centers for the 2-D r-z region in Eq. (18), as well as at centers of cell-edge boundaries of the 2-D region. Flux moments files are then saved for use for one or more subsequent secondary 3-D problems.

(ii) Carry out the spatial transformations in Eqs. (15) and (16) for each of pre-selected boundaries of a secondary 3-D problem, to convert the coordinates of the geometric centers of mesh-cell faces from the 3-D coordinate system to the corresponding 2-D r-z coordinate system. Perform linear spatial interpolations to evaluate full ϕ_{nm} or partial ϕ^{+}_{nm} and ϕ^{-}_{nm} flux moments at centers of mesh cell faces of the 3-D problem. This step can be highly vectorized or parallelized as was done in our work on the 3-D to 3-D splice option [1].

(iii) Carry out the angular transformation in Eq. (17) for directions incident at the geometric centers of mesh-cell faces to convert the 3-D angular quadrature from the 3-D coordinate system to the corresponding 2-D r-z coordinate system. Apply the spherical harmonics expansion in Eq. (19) to evaluate incident fluxes at centers of mesh cell faces of the 3-D problem. Again, this step can be highly vectorized or parallelized.

In rare situations where the angular quadratures for the 2-D primary problem and the 3-D secondary problem are identical, and where the bottom (top) boundary of the 3-D problem lies along a border of the region of the 2-D problem specified in Eq. (18), the actual angular fluxes should be saved on the bottom (top) boundary of the region of the 2-D problem in place of flux moments. No angular interpolation will be needed at this bottom (top) boundary.

Note that boundaries of the 3-D problem may extend beyond the space of a primary 2-D problem. Incident angular fluxes are set to zero on portions of a boundary outside the space of the 2-D problem.

5. Sample Application

The cylinder model problem shown in Figure 2 was developed to test the accuracy of the 2-D to 3-D splice technique. The model initially had a 48" radius and 40" height, with a source region in the lower left hand corner, surrounded by regions of water, iron and air. Flux moment data was saved in the bounded region of Figure 2 which is labeled "1st 3-D Boundary." These fluxes were then used to construct boundary angular fluxes on all six faces of a 3-D problem corresponding to the bounded region in Figure 2. A radial cross section of this 3-D geometry is shown in Figure 3. This model was built with dimensions 18" by 48" by 18". Integrated fluxes were then generated over the various material regions in this problem. A corresponding 3-D model of the entire cylinder was also developed, having the dimensions of 48" by 48" by 40". The model was built using rectangular x-y-z coordinates; so approximations due to stepping of the curved surfaces was necessary. Edits were built into this 3-D full model to correspond to the 18" by 48" by 18" region solved using the splice method. The regions being compared were identical in material composition and volume. The differences were in the fact that in one case, the source was based on the volumetric source built into the lower left hand corner of the 3-D representation of the cylinder, and in the other case, the source was based on the angular fluxes generated at each of the six faces from the r-z cylindrical model. In each case, two splice models and two 3-D models were generated over the same physical dimensions. One model used 1" mesh everywhere, and the second one used 0.5" mesh everywhere. Comparisons of integrated flux results showed that mesh refinement improved the agreement between the full and spliced 3-D models. The agreement was also better for regions nearer to the source. In the iron region nearest to the source, the agreement in group 7 of an 11 energy group structure [1] improved from 12.8% to 2.0%. In the same group, for the water region furthest from the source, the agreement improved from 17.0% to 5.5%. Comparisons for the other regions were similar. Agreement was also slightly better at the higher energy groups. In the cylindrical geometry model, a 46 angles per octant angular quadrature was used. In each of the 3-D models, both S-16 and a variation on a 46 angles per octant quadrature were used. It is not possible to have identical quadratures in 2-D cylindrical and 3-D rectangular geometry models.

A subset of the model in Fig. 3 corresponding to a splice region with a single material was built with dimensions 8" by 10" by 5". Here, the boundaries can be represented exactly and there is no need for a stepped up rectangular representation. The difference between integrated fluxes for group 1 over the homogenous splice and over the corresponding region of the 3-D full model

dropped to around 3%. The entire models were then shrunk by using dimensions in centimeters rather than in inches. The integrated fluxes now agreed to under 1%.

A final comparison between point-wise angular fluxes at the centers of mesh cell of the 3-D homogeneous splice and corresponding locations of the 2-D cylindrical problem computed based on linear interpolations. The differences are summarized in Table 1

Table 1: Differences Between 3-D Homogenous Splice and Corresponding 2-D Flux Results

Mesh Plane	1	2	3	4	5
pointwise	.03-1.42%	.01-1.36%	.01-1.99%	.05-2.50%	.00-2.27%
integrated	0.64%	0.56%	0.68%	1.16	1.20%

A second simple benchmark model problem is provided here to demonstrate the coupling technique. Figure 4 displays an elevational view of a 2-D cylindrical geometry model of the primary portion of the calculation. The 2-D model has a fuel region surrounded by water contained within a pressure vessel. The vessel is surrounded by a primary shield which includes metal shielding on the interior and neutron shielding on the outer portion of the shield. Figure 5 shows a model splice through a cross section of a reactor nozzle/shield penetration. A 2-D cylindrical discrete ordinates calculation for the geometry in Figure 5 would not be appropriate because the localized nozzle and penetration geometry would have to be rotated 360 degrees, magnifying the horizontal nozzle streaming path and unrealistically closing off the vertical streaming path. The region over which the boundary fluxes are determined for the 3-D problem is shown by a rectangle on Figure 4. The boxed region represents the location of the vessel nozzle and associated streaming annulus. The "no-nozzle" 2-D geometry is used and the lower boundary chosen such that the dominant neutron streaming path input to the 3-D problem is unaffected by the presence of the nozzle. Two dimensional calculations with and without the nozzle geometry are compared to aid in locating the lower splice boundary. Two-dimensional r-z flux results (not shown for brevity) in the form of constant neutron flux lines superimposed on the outline geometry plots of Figures 4 and 5 for the no-nozzle and nozzle geometries were used to determine the location of the lower boundary of the splice region.

The discrete ordinates solution for the 2-D model had 35,000 mesh blocks and 166 angles per octant (664 total angular directions). The 3-D model covering the nozzle penetration region had one million mesh cells and employed 100 angles per octant (800 total angular directions) in the discrete ordinates solution. The large numbers of angular directions were chosen to avoid ray effects and to properly account for the expected varying streaming paths.

Figure 6 provides two views of the 3-D splice with flux isosurfaces showing the expected multidimensionality of streaming through the gaps. In our experience, computing and showing accurate flux levels at different locations around nozzles would not have been possible with previous combinations of 2-D models.

Solutions of large 3-D transport problems are still very expensive and a 3-D model of the full configuration in Figure 5 would have been prohibitive. The 2-D to 3-D splice option has been demonstrated to be an invaluable tool that ensures neutron shielding will be properly sized to meet radiation objectives.

ACKNOWLEDGMENTS

This work was supported by the U.S. Department of Energy under Contract DE-AC11-93PN38195.

REFERENCES

1. I. K. Abu-Shumays and C. E. Yehnert, "Angular Interpolations and Splice Options for Three–Dimensional Transport Computations," in Proceedings of ANS 1996 Topical Meeting on "Radiation Protection and Shielding," Vol. 1, pp. 373-383, No. Falmouth, Massachusetts, April 21-25, 1996.

2. E. Anderson, et al., LAPACK Users' Guide, SIAM, Philadelphia, Pennsylvania (1992).

3. J. J. Dongarra, C. B. Moler, J. R. Bunch and G. H. Stewart, LINPACK Users' Guide, SIAM, Philadelphia, Pennsylvania (1979).

4. W. A. Rhoades and R. L. Childs, "An Updated Version of the DOT 4 One-and Two-Dimensional Neutron/Photon Transport Code," ORNL-5851, Oak Ridge National Laboratory (1982).

5. W. A. Rhoades and R. L. Childs, "The TORT Three-Dimensional Discrete Ordinates Neutron/ Photon Transport Code," ORNL-6268, Oak Ridge National Laboratory (1987).

6. D. B. Simpson, "Splicing and Bootstrapping Methods for Coupling Primary DORT/TORT Models to Secondary TORT Models," in Proceedings, December 2-3, 1996 meeting on "3-D Deterministic Radiation Transport Computer Programs - Features, Applications and Perspectives," Nuclear Energy Agency, Organization for Economic Co-operation and Development (OECD), Paris, France, 1997

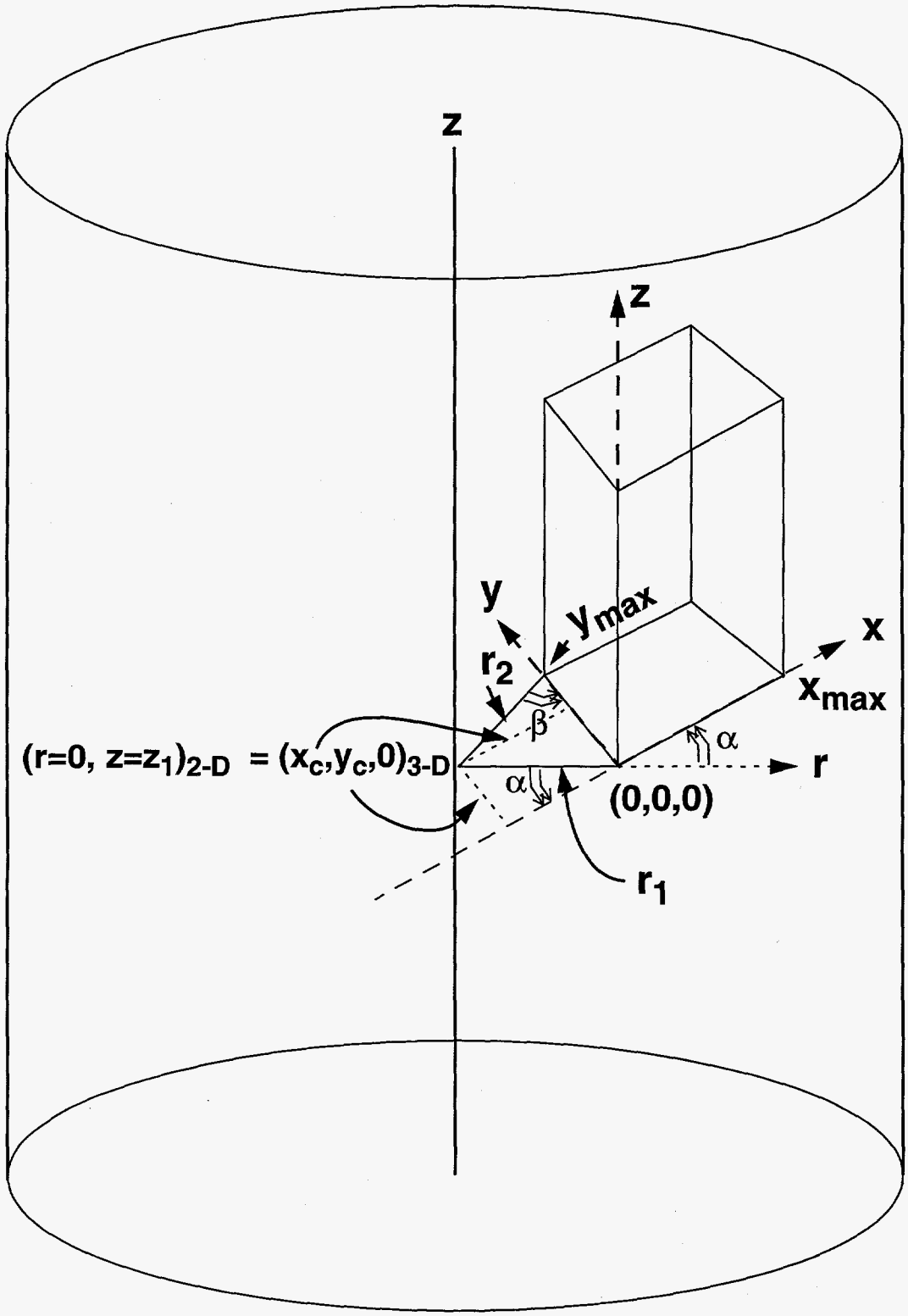

FIGURE 1. 2-D R-Z CYLINDRICAL PRIMARY SOLUTION SPACE WITH A 3-D SECONDARY SOLUTION SPACE EMBEDDED IN IT.

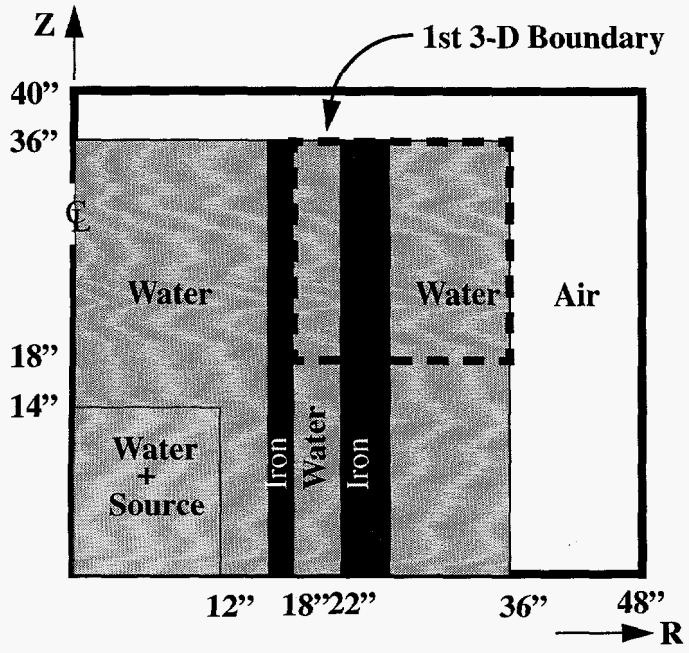

Figure 2.

Cylindrical Geometry Model for 3-D Test

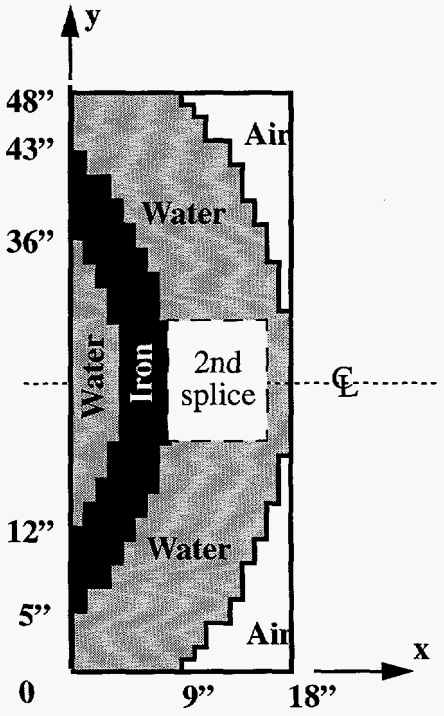

Figure 3.

Radial Slice from 3-D Cylinder Model

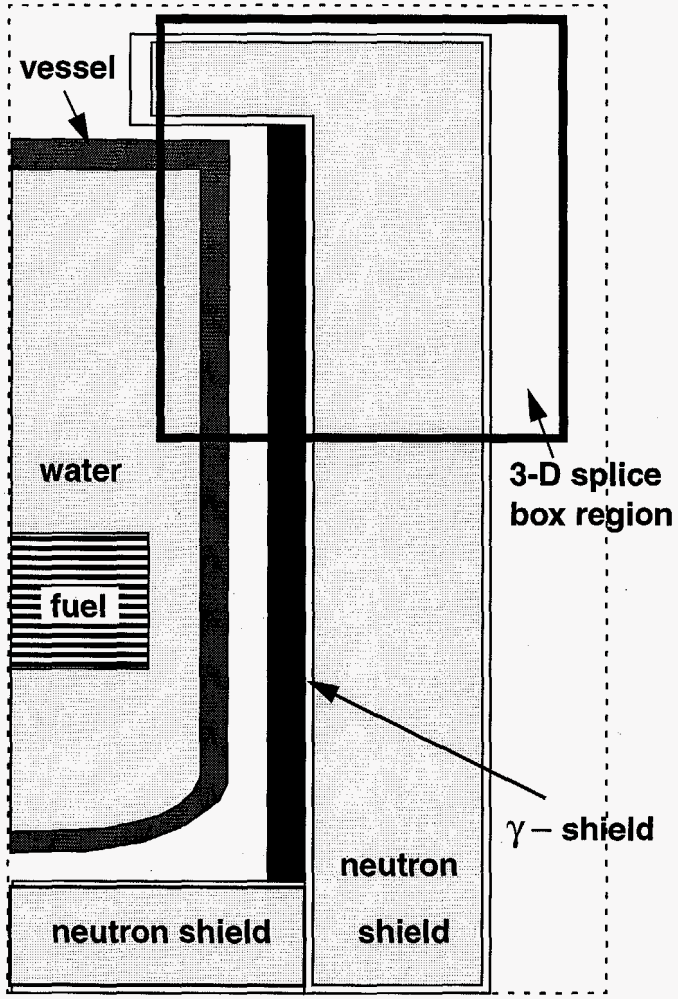

Figure 4. Simple 2-D Reactor Model

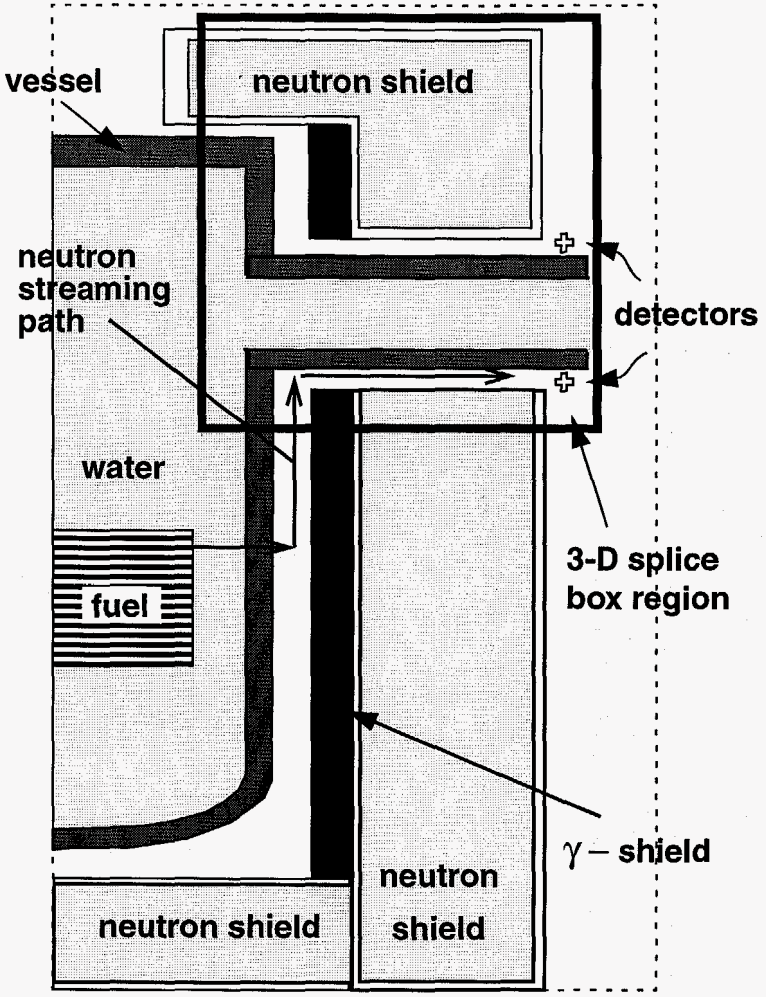

Figure 5. Simple 2-D Reactor Model with 3-D Nozzle

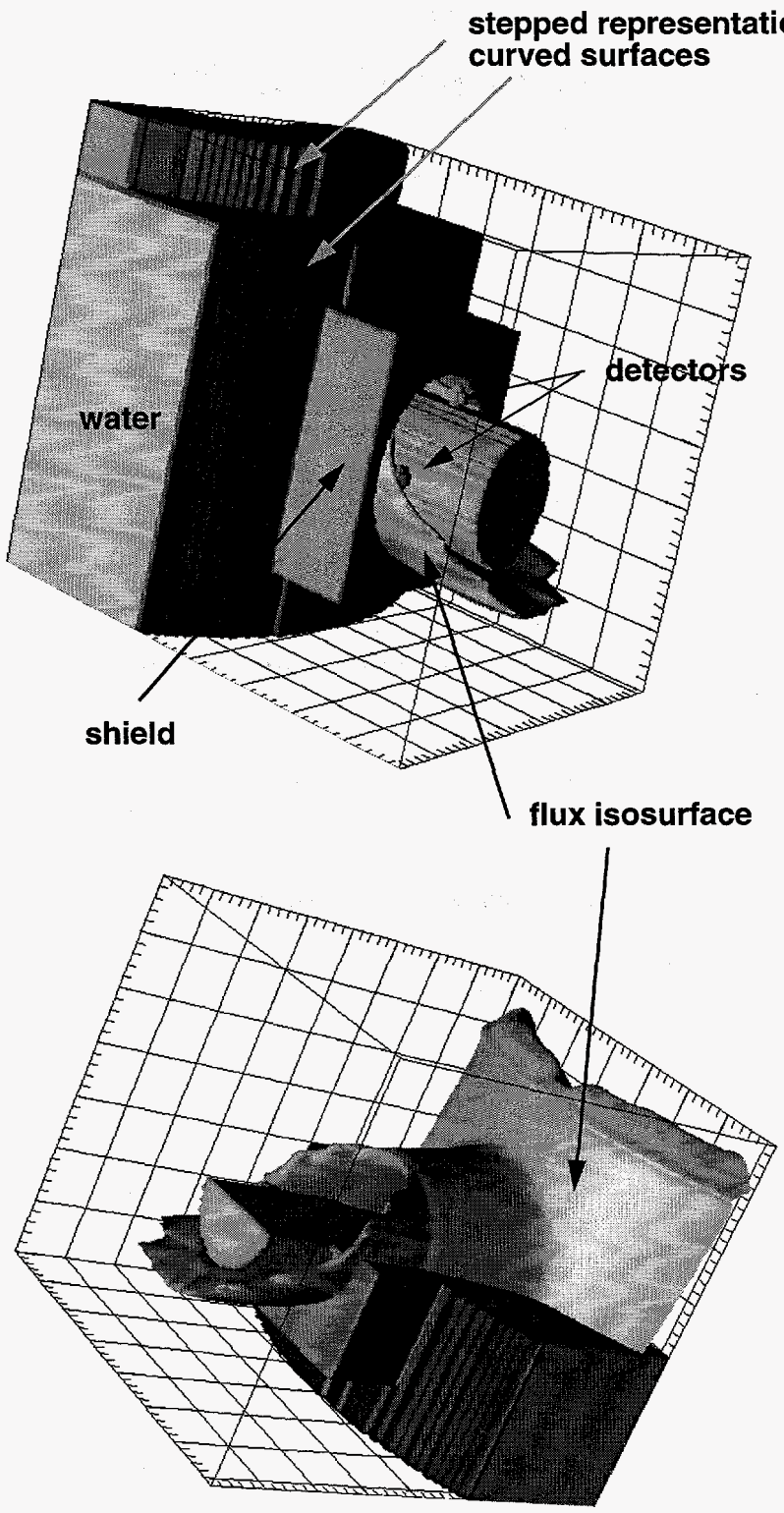

Figure 6. Three-Dimensional Geometry Model and Flux Isosurface